Sensitivity of Antarctic shelf waters and abyssal overturning to local winds

Adele K. Morrison,[a] Wilma G. C. Huneke,[b] Julia Neme,[c] Paul Spence,[d] Andrew McC. Hogg,[b] Matthew H. England,[c] and Stephen M. Griffies[e]

[a] *Research School of Earth Sciences and Australian Centre for Excellence in Antarctic Science, Australian National University, Canberra, Australia.*

[b] *Research School of Earth Sciences and ARC Centre of Excellence for Climate Extremes, Australian National University, Canberra, Australia.*

[c] *Climate Change Research Centre, Centre for Marine Science and Innovation (CMSI), and Australian Centre for Excellence in Antarctic Science, University of New South Wales, Sydney, Australia.*

[d] *Institute for Marine and Antarctic Studies and Australian Centre for Excellence in Antarctic Science and Australian Antarctic Partnership Program, University of Tasmania, Hobart, Australia.*

[e] *NOAA Geophysical Fluid Dynamics Laboratory and Princeton University Program in Atmospheric and Oceanic Sciences, Princeton, NJ, USA.*

Corresponding author: Adele Morrison, Adele.Morrison@anu.edu.au

Early Online Release: This preliminary version has been accepted for publication in *Journal of Climate*, may be fully cited, and has been assigned DOI 10.1175/JCLI-D-22-0858.1. The final typeset copyedited article will replace the EOR at the above DOI when it is published.

ABSTRACT: Winds around the Antarctic continental margin are known to exert a strong control on the local ocean stratification and circulation. However, past work has largely focused on the ocean response to changing winds in limited regional sectors and the circumpolar dynamical response to polar wind change remains uncertain. In this work, we use a high-resolution global ocean - sea ice model to investigate how Dense Shelf Water formation and the temperature of continental shelf waters respond to changes in the zonal and meridional components of the polar surface winds. Increasing the zonal easterly wind component drives an enhanced southward Ekman transport in the surface layer, raising sea level over the continental shelf and deepening coastal isopycnals. The downward isopycnal movement cools the continental shelf, as colder surface waters replace warmer waters below. However, in this model the zonal easterly winds do not impact the strength of the abyssal overturning circulation, in contrast to past idealised model studies. Instead, increasing the meridional wind speed strengthens the abyssal overturning circulation via a sea ice advection mechanism. Enhanced offshore meridional wind speed increases the northward export of sea ice, resulting in decreased sea ice thickness over the continental shelf. The reduction in sea ice coverage leads to increased air-sea heat loss, sea ice formation, brine rejection, Dense Shelf Water formation and abyssal overturning circulation. Increasing the meridional winds causes warming at depth over most of the continental shelf, due to a heat advection feedback associated with the enhanced overturning circulation.

Accepted for publication in *Journal of Climate*. DOI 10.1175/JCLI-D-22-0858.1.

1. Introduction

Ocean circulation around the Antarctic margin is fundamentally important for regulating the temperature of waters that interact with Antarctica's ice shelves and marine terminating ice sheets, with implications for global sea level rise. Several factors control the flow of water on the Antarctic continental shelf, including buoyancy fluxes, local winds, tides, and other remote forcings, such as teleconnections from the tropics and changes in the subpolar westerly winds (e.g. Frankcombe et al. 2013; Spence et al. 2014; Palóczy et al. 2018; Lago and England 2019; Holland et al. 2019; Moorman et al. 2020; Bowen et al. 2021; Beadling et al. 2022; Tesdal et al. 2023). Little is known about how the circumpolar Antarctic shelf waters and abyssal overturning circulation respond to the near-Antarctic surface winds, with most studies focusing on the westerly wind belt to the north (e.g. Spence et al. 2014), or regional case studies (e.g. Naughten et al. 2022). The goal of this study is to examine the circumpolar response of shelf water properties and the abyssal overturning circulation to changes in the polar wind field, south of the westerlies.

The climatological mean winds around the Antarctic continental margin are characterized by particularly strong easterly winds around the eastern Antarctic sector, weaker easterlies around the West Antarctic sector, and mostly offshore (southerly) winds flowing off the continent (Fig. 1). The wind field advects sea ice away from the coast, creating coastal polynyas that leave the open ocean exposed to strong water-mass transformation and resulting in Dense Shelf Water (DSW) formation (Bromwich and Kurtz 1984; Massom et al. 1998; Mathiot et al. 2010). The polar easterlies drive onshore surface Ekman transport, which creates a wedge of cold fresh Antarctic Surface Water separated from warm Circumpolar Deep Water (CDW) around much of the continent. The stronger the easterly wind field, the stronger this stratification of water masses, resulting in the Antarctic Slope Front and via geostrophic adjustment, the Antarctic Slope Current (Thompson et al. 2018). A strong Antarctic Slope Front is conducive to protecting Antarctica's ice shelves from intrusions of warm CDW, but it is wind dependent, with regional sectors that exhibit weaker winds more prone to warm CDW intrusions (e.g. the Amundsen and Bellingshausen Seas; Schmidtko et al. (2014)). The wind field over the Antarctic margin also controls surface buoyancy fluxes, by driving the formation and advection of sea ice (Pellichero et al. 2018). Any changes in the polar winds thus have the potential to fundamentally change Antarctic sea-ice coverage, DSW formation and the abyssal overturning circulation, and hydrographic properties on the shelf.

Accepted for publication in *Journal of Climate*. DOI 10.1175/JCLI-D-22-0858.1.

Observations of wind trends and variability around the Antarctic margin rely on sparse measurements, and different reanalysis products disagree on the magnitude and sign of historical trends (Hazel and Stewart 2019; Neme et al. 2022). Future projections across early generation CMIP models suggest a weakening of the coastal easterlies during austral summer and autumn, particularly around East Antarctica, associated with the poleward migration of the westerlies (Bracegirdle et al. 2008). A more recent analysis suggests that a circumpolar weakening of both the zonal and meridional near-Antarctic winds is robust in CMIP6 model projections, with a 23% reduction in zonal wind speed and a 7% reduction in meridional wind speed under a high emission scenario (Neme et al. 2022). More generally there is significant interannual - multi-decadal variability in the winds around the Antarctic margin (Neme et al. 2022), due to both tropical variability and teleconnections, and variability in the Southern Annular Mode (e.g. Fogt and Bromwich 2006; Bracegirdle et al. 2008; Raphael et al. 2016). Given this strong variability alongside projected trends, it is important to understand the response of the Antarctic shelf circulation and hydrography to both increases and decreases in the local winds.

Past studies have highlighted several different dynamical mechanisms by which the near-Antarctic winds impact the ocean circulation and properties around the Antarctic margins. We first discuss studies that have focused on dynamics associated with the zonal component of the winds. Increasing the zonal easterlies enhances the surface southward Ekman transport, resulting in coastal Ekman downwelling and a downward shift of the isopycnals over the continental shelf. This deepening of isopycnals drives a cooling of shelf waters, as cold upper ocean waters replace warmer waters at depth (Spence et al. 2014). Stewart and Thompson (2012) showed in an idealised model configuration that the abyssal overturning circulation also increases with strengthened easterly winds, driven in part by the increase in the southward surface Ekman transport and the enhanced upwelling of CDW. An increase in overturning also requires a change in water mass transformation, which in the idealised setup of Stewart and Thompson (2012) likely occurred via a change in the heat flux from surface temperature restoring. It is possible that a more complex representation of buoyancy forcing (i.e. as arising from dynamic sea ice) could alter the response of the abyssal overturning to increasing zonal winds. Others have proposed a more local wind control mechanism, whereby increasing easterlies enhance the geostrophic outflow of DSW through cross-shelf troughs, through a deepening of the Antarctic Slope Front that alters the inflow of lighter waters across the

Accepted for publication in *Journal of Climate*. DOI 10.1175/JCLI-D-22-0858.1.

shelf-break (Kida 2011; Wang et al. 2012). A sea-ice driven mechanism has also been identified, whereby reduced zonal winds upstream (to the east) of dense water formation regions lead to a reduction in sea ice advection westward, more open water area and increased sea ice and dense water formation (Silvano et al. 2020; Schmidt et al. 2023). Finally, the ocean temperature and ice shelf melting in the Amundsen Sea have been shown to be sensitive to the local easterly winds at the shelf break; over monthly to interannual timescales (Silvano et al. 2022), increasing easterly winds in this region reduce the undercurrent on the slope and thereby decrease the on-shelf transport of CDW through troughs (e.g. Jenkins et al. 2016; Caillet et al. 2023).

Fewer studies have focused on the response of the ocean circulation and properties to changes in the meridional component of the near-Antarctic winds. However, one wind-driven sea ice advection mechanism stands out from regional studies focused on the Weddell and Ross Seas. Several modelling and observational studies have found that under increased meridional winds, there is an anomalous northward export of sea ice away from the coast that reduces the sea ice concentration over the shelf and leads to an enhancement of DSW formation (Timmermann et al. 2002; McKee et al. 2011; Dinniman et al. 2018; Hazel and Stewart 2020).

In summary, from CMIP6 projections, we expect a weakening of the near-Antarctic winds over the 21st century. However, past work on the response of the ocean properties and circulation around the Antarctic margins to winds has largely focused on limited regional sectors and there remains considerable uncertainty around the circumpolar dynamical response to winds. In particular, there are several competing dynamical theories to explain the sensitivity of the abyssal overturning circulation to wind change (e.g. Stewart and Thompson 2012; Kida 2011; McKee et al. 2011). In this paper we aim to investigate the circumpolar response of the shelf waters and the abyssal overturning to changing near-Antarctic winds.

2. Methods

This study uses the Australian Community Climate and Earth System Simulator Ocean Model (ACCESS-OM2-01; Kiss et al. 2020), a global ocean-sea ice model with a horizontal grid spacing of 0.1°, and 75 vertical z* levels. The model's ocean component is MOM5.1 (Griffies 2012), and is coupled to the CICE5.1.2 sea ice model (Hunke et al. 2015). The model does not include ice shelf cavities or tides. The model is forced with a prescribed atmospheric forcing from JRA55-do

Accepted for publication in *Journal of Climate*. DOI 10.1175/JCLI-D-22-0858.1.

(Tsujino et al. 2018), and sea surface salinity is restored to a World Ocean Atlas climatology, as detailed in Kiss et al. (2020). A 12-month period (from May 1990 to April 1991) from JRA55-do (version 1.3) was looped repeatedly to drive the CONTROL simulation used in this work, with the forcing year chosen due to the neutral state of several climate indices (e.g. El Niño-Southern Oscillation, Southern Annular Mode; Stewart et al. 2020). The repeat year forcing provides a very stable CONTROL configuration with no interannual atmospheric forcing variability from which perturbation experiments are branched off. JRA55-do wind velocities (on a 0.5° grid) are interpolated on to the model grid using a smooth ('patch') interpolation method, with no special treatment near land. The CONTROL simulation was spun up for 250 years prior to the 10 year analysis period used in this study.

The CONTROL simulation compares generally well with observations. The overall distribution of water masses is fairly represented, although the simulated water masses are fresher and colder compared with World Ocean Atlas observations (Locarnini et al. 2018; Zweng et al. 2019) along the shelf break (Fig. S1) and with Schmidtko et al. (2014) at the bottom of the continental shelf (Fig. S2). The simulated winter sea ice extent is close to NOAA/NSIDC satellite observations (Peng et al. 2013; Meier et al. 2017) with some larger biases during summer when the model underestimates the sea ice coverage (Fig. S3). Most notably for a global model, ACCESS-OM2-01 forms dense water on the Antarctic continental shelf that descends all the way to the abyss (Solodoch et al. 2022). The dense water export across the shelf break in the model (9.0 Sv; Fig. 2 and Fig. S4) aligns well with the observational estimate of 8.1 ± 2.6 Sv (Orsi et al. 2002).

Perturbations to the surface wind fields were applied in order to assess the sensitivity of the Antarctic margins to wind amplitude, Table 1. The two main perturbation simulations used in this study are WIND+ and WIND-, and are respectively forced by increased and decreased near Antarctic winds by 10% (both zonal and meridional components). The perturbation to the wind field was applied south of the dividing line between the annual average easterly and westerly winds (blue line shown in Fig. 1a). The dividing line was constructed by following the minimum in the absolute value of the annual average JRA55-do wind speed used to drive the CONTROL simulation. As shown in Fig. 1a, this definition closely tracks the divide between the easterly and westerly winds. We perturb the wind south of the dividing line by adding/subtracting 10% of the rolling monthly mean zonal and meridional wind velocities to the original 3-hourly forcing

Accepted for publication in *Journal of Climate*. DOI 10.1175/JCLI-D-22-0858.1.

fields. By using the rolling monthly mean for the perturbation, rather than directly scaling the 3-hourly fields or adding a fraction of the annual mean winds, we ensure that we are not amplifying the storm activity and that there are minimal changes to the seasonal cycle. For example, the easterlies used to force the CONTROL simulation are stronger in winter and weaker in summer and therefore adding/subtracting a constant fraction of the annual wind velocities (rather than rolling monthly mean wind velocities as we use here), would inadvertently be overly strengthening the summer winds compared to the winter winds. Two additional simulations were carried out in order to study the separate effects of the zonal and meridional components of the wind field in the WIND+ experiment. In these simulations, the perturbation was applied to the zonal (WIND+$_{\text{zonal}}$) and meridional (WIND+$_{\text{merid}}$) components separately. A final simulation (WIND+$_{\text{no\_local}}$) was designed to address the sensitivity of DSW formation to local katabatic winds. ACCESS-OM2 has a representation of DSW formation processes and regions consistent with observations, with four main formation regions in the Weddell and Ross seas, Adelie Coast and Prydz Bay (see Fig. 4a). Therefore, in this perturbation, the wind amplitude anomaly was applied everywhere south of the dividing line except in the DSW production regions (i.e. the yellow boxes shown in Fig. 1a).

TABLE 1. Summary of the perturbation simulations analysed in this study. All perturbations were applied to the surface wind field in the region south of the zero wind speed line (blue contour in Fig 1a).

Simulation	Description
WIND+	+10% applied to surface wind velocities
WIND-	-10% applied to surface wind velocities
WIND+$_{\text{zonal}}$	+10% applied to zonal wind velocities
WIND+$_{\text{merid}}$	+10% applied to meridional wind velocities
WIND+$_{\text{no\_local}}$	As in WIND+, except no perturbation is applied in the DSW formation regions (yellow boxes in Fig. 1a)

3. Results

a. Sea level and dense water response

The initial response to an increase in wind magnitude around the Antarctic continent is higher sea level over the continental shelf (WIND+ experiment, Fig. 2a), as expected from the enhanced onshore Ekman transport. This behavior is seen soon after the perturbation is applied in the WIND+ experiment, with the initial anomaly in sea level reaching nearly 0.5 m, averaged over the

Accepted for publication in *Journal of Climate*. DOI 10.1175/JCLI-D-22-0858.1.

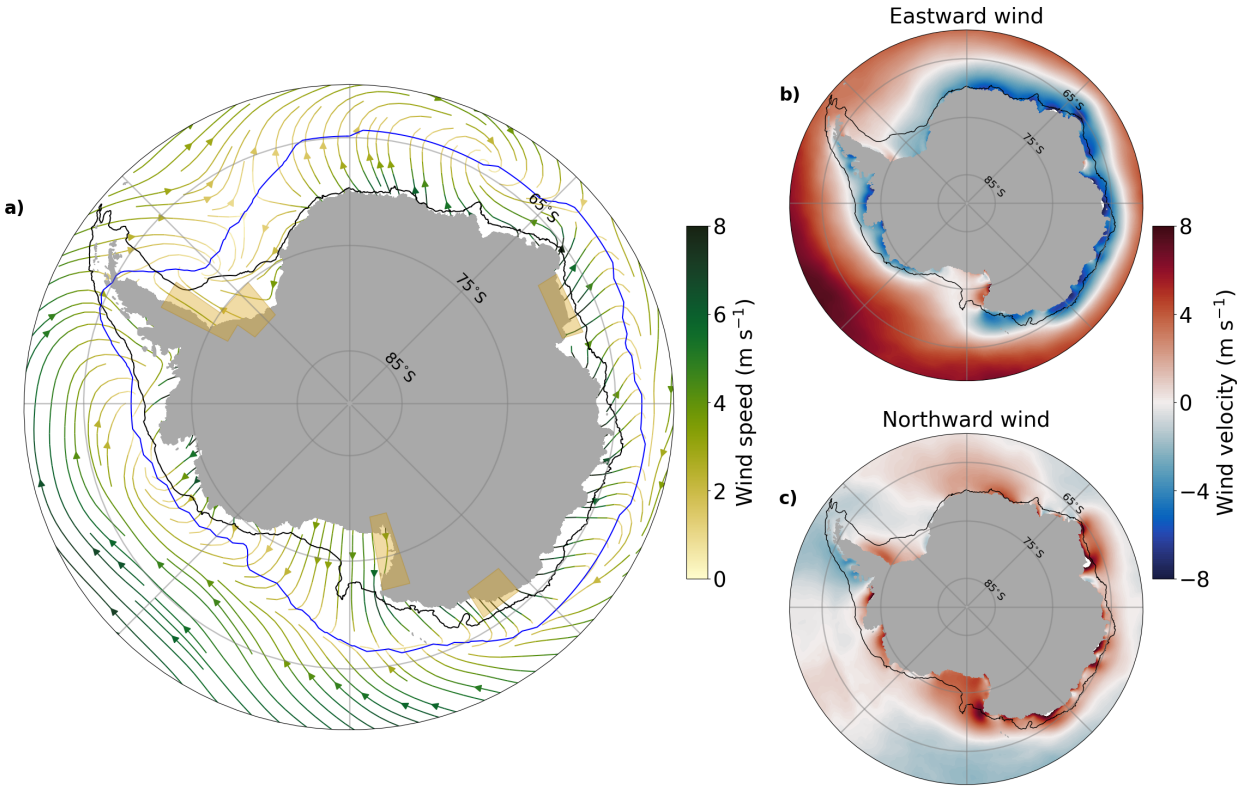

FIG. 1. a) CONTROL time mean surface wind streamlines colored by wind speed. Wind amplitude was altered in the region south of the blue line, which is aligned with the minimum in wind speed and closely tracks the separation of westerly and easterly winds. Yellow boxes show the regions where the wind anomaly was not applied in the WIND+$_{\text{no\_local}}$ perturbation. b) CONTROL zonal wind velocity (westward is positive). c) CONTROL meridional wind velocity. In all panels the thin black contour shows the 1000 m isobath and gray lines are lines of latitude and longitude.

continental shelf. The sea level response in the WIND- perturbation is not quite symmetric about the control, but is still persistently negative over the first 2 years, consistent with reduced onshore Ekman transport when the wind amplitude is reduced. However, beyond the second year in both perturbations, the initial sea level response is reversed, with opposite sign anomalies continuing to grow over the 10 years of the simulation.

We hypothesise that the deviation of the sea level response from the expected Ekman dynamics after the second year is driven by steric sea level change arising from changing water masses on the continental shelf and in the abyss. The longer-term decrease in sea level in the WIND+ perturbation would be consistent with increased density in the water masses on the continental shelf, which we

Accepted for publication in *Journal of Climate*. DOI 10.1175/JCLI-D-22-0858.1.

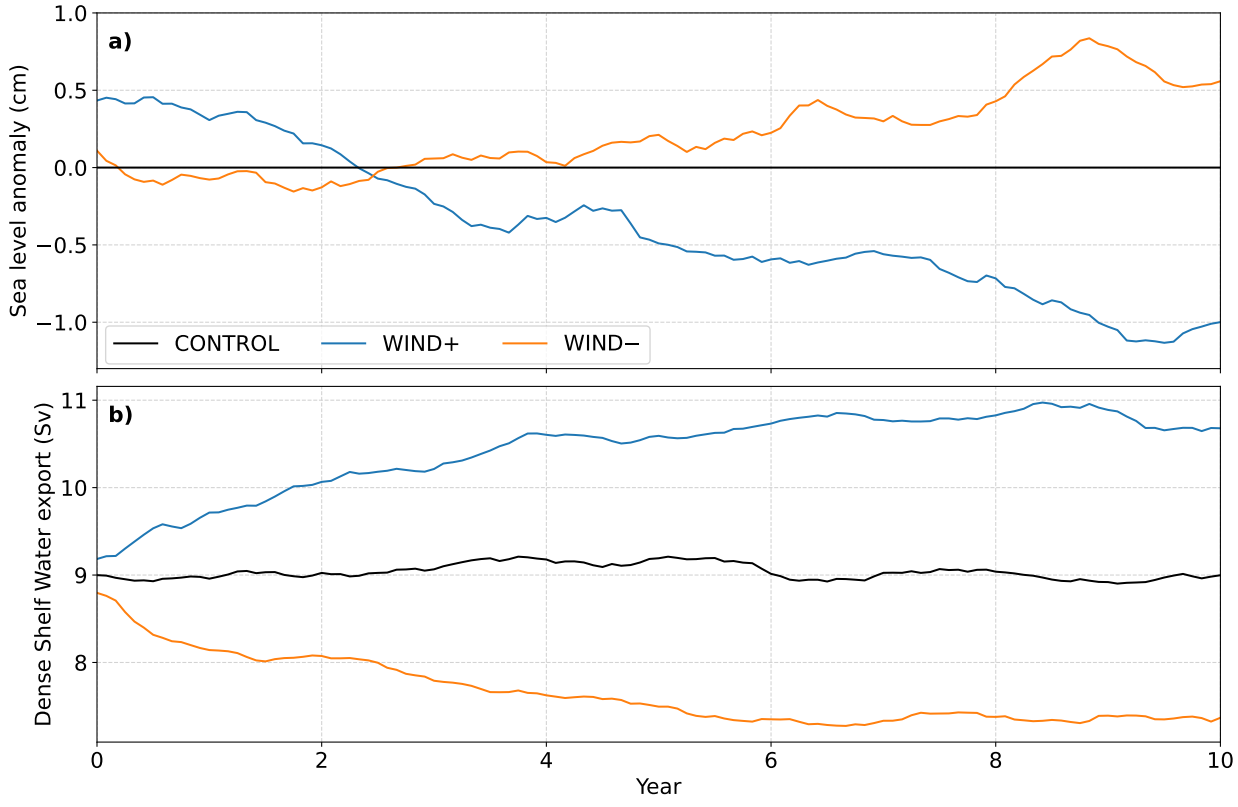

FIG. 2. a) Sea level anomaly relative to the CONTROL (black), averaged over the continental shelf for the WIND+ (blue) and WIND- (orange) simulations, with a 12-month running mean applied. b) Dense Shelf Water export across the 1000 m isobath, summed circumpolarly around Antarctica, for the CONTROL (black), WIND+ (blue) and WIND- (orange) simulations.

would also expect to drive more DSW export from the shelf. Here we define DSW export to be the equatorward transport across the 1000 m isobath, first integrated along the isobath and then summed cumulatively across density layers from the densest layer up to the density layer where the transport begins to reverse. An analysis of the DSW export across the 1000 m isobath shows that indeed more dense water is formed and exported northward across the continental slope following an increase in wind amplitude, with a symmetric response (i.e. decrease in DSW export) in the WIND- perturbation (Fig. 2b). Over the 10 year simulation, DSW export changes by ±18% in the perturbation experiments. The depth profile of the overturning streamfunction at the 1000 m isobath is shown in Fig. S4.

Accepted for publication in *Journal of Climate*. DOI 10.1175/JCLI-D-22-0858.1.

The impact of changing DSW export can be explored by looking at the ideal age in the deepest model cell. Ideal age is a passive tracer that is set to zero at the ocean surface and increases at a rate of 1 year per year in the ocean interior. Bottom age decreases when there is higher DSW export from the shelf, as these waters have recently been ventilated and are therefore younger. There is considerable spatial complexity in the ocean age response to changing wind amplitude (Fig. 3a,b). The primary response in the WIND+ case is an increase in DSW formation, enhanced AABW transport and a consequent decrease in ideal age in the abyssal ocean (Fig. 3a). The decrease in abyssal age in the WIND+ perturbation is widespread, except for the open ocean adjacent to West Antarctica, where there is no DSW formation or export. The Weddell Sea AABW export pathway is particularly pronounced, following the continental slope along the western and then northern edges of the Weddell Gyre. Widespread regions of the continental shelf become younger following the increase in wind amplitude, in particular the Amundsen Sea and East Antarctica between the Ross Sea and Prydz Bay. This decrease in age on the shelf is consistent with the expected response from the increased poleward surface Ekman transport, which drives a downward shift of isopycnals and shifts younger upper ocean waters deeper in the water column. Within the DSW formation regions (yellow boxes in Fig. 3a), the bottom age anomaly is close to zero, because these waters are already ventilated in the CONTROL run and therefore have an age close to zero. However, on the continental shelf downstream (westward) of the Weddell and Cape Darnley DSW formation regions, there is an increase in age, which results from the reduced along-shelf connectivity driven by the increase in DSW overflow transport (Moorman et al. 2020).

The response on the shelf between the WIND+ and WIND- cases is largely symmetric about the control. For the remainder of the results section, for simplicity we will focus on one perturbation case, the WIND+ experiment. Given that future projections suggest a weakening of the polar winds (Neme et al. 2022), we will also discuss the implications of the dynamics we identify for the WIND+ case for a future weakening wind scenario.

The bottom shelf waters become more saline around most of the continent in the WIND+ perturbation (Fig. 3c), as expected from the increased formation rate of DSW. This increase in salinity, and therefore density, over the continental shelf in the WIND+ perturbation is consistent with the long-timescale decrease in sea level (Fig. 2a). A decomposition of the sea level changes into steric and mass contributions (following Griffies et al. 2014) however reveals slightly more

Accepted for publication in *Journal of Climate*. DOI 10.1175/JCLI-D-22-0858.1.

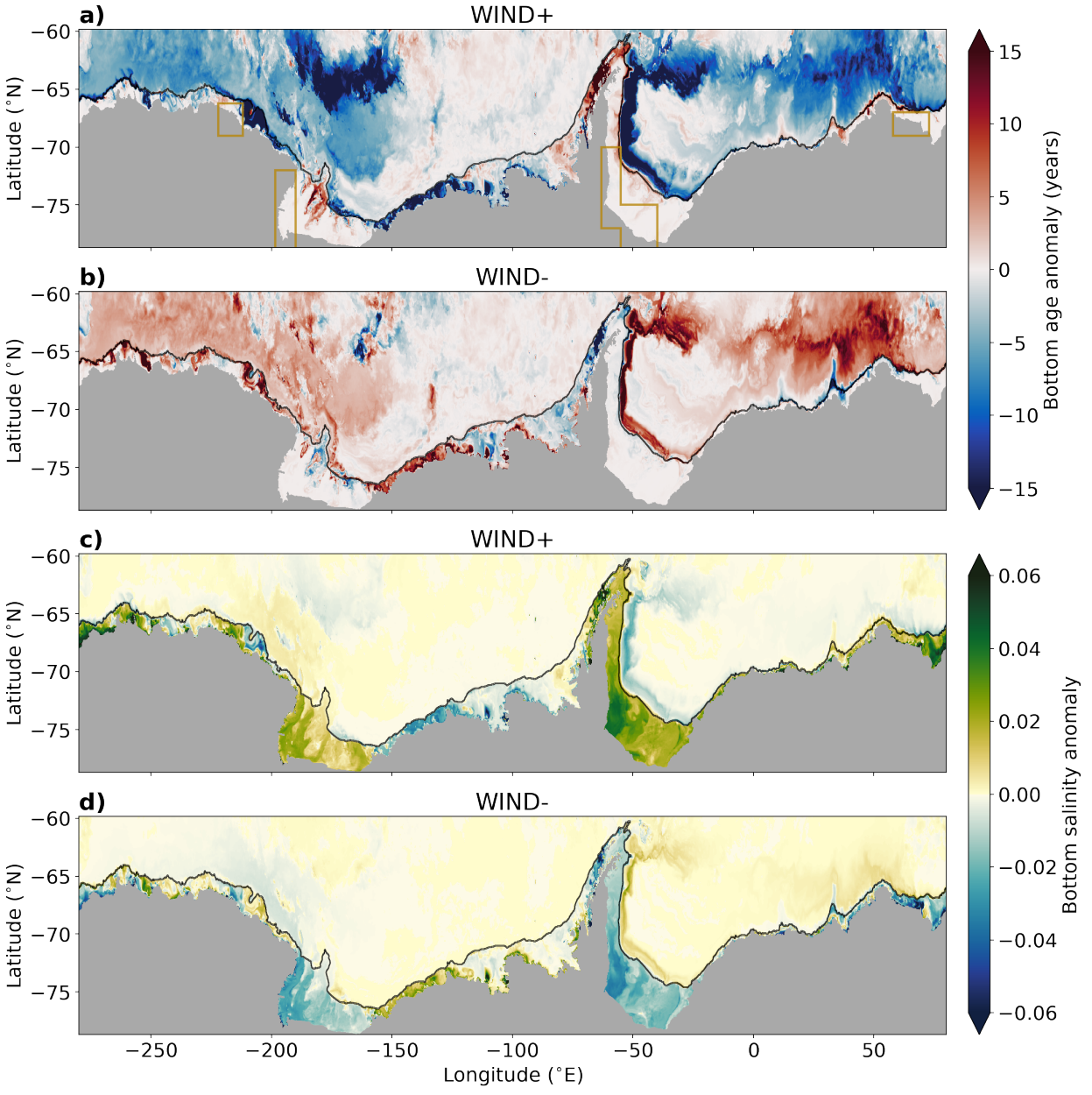

FIG. 3. Bottom age tracer anomaly in the a) WIND+ and b) WIND- perturbation, averaged over year 10 of the simulation. Yellow boxes in a) indicate the DSW formation sites. Bottom salinity anomaly in c) WIND+ and d) WIND-, averaged over years 6 to 10 of the simulation. The black contour is the 1000-m isobath and separates the continental shelf from the open ocean.

complex dynamics: the decrease in sea level over the shelf in the WIND+ case has significant contributions from both the steric and mass terms (not shown). In the WIND+ perturbation, waters

Accepted for publication in *Journal of Climate*. DOI 10.1175/JCLI-D-22-0858.1.

become denser both over the shelf and in the abyss, decreasing steric sea level over a wide region of the Southern Ocean, south of the Antarctic Circumpolar Current. The steric decrease in the open ocean is larger than over the shelf, due to the thicker bottom water layer in the abyss. As explained in Griffies et al. (2014), the resulting change in cross-slope gradient in steric sea level drives a mass redistribution, with mass flowing off the shelf to re-balance the cross-slope gradient in sea level that is set up by the dense water-driven changes in steric sea level.

The Amundsen Sea continental shelf region is an exception to the widespread salinification; instead the waters there become fresher in the lower water column in the WIND+ case. Fresher and younger (Fig. 3a) waters in the Amundsen region are indicative of enhanced local ventilation. Mixed layer depths in the Amundsen region also increase (not shown), driven by locally stronger winds in the WIND+ perturbation.

Because the age and salinity changes over much of the shelf are driven by DSW changes, we now investigate the mechanism driving the increase in DSW formation in the WIND+ case.

We formulate three hypotheses to explain the increased DSW formation:

1. The WIND+ experiment has enhanced katabatic winds, which increase the surface water mass transformation in specific locations where coastal polynyas allow production of DSW.

2. The WIND+ experimental forcing acts to increase Ekman driven upwelling, increasing along-isopycnal transport in CDW layers and thus bringing more salt onto the continental shelf. This small change in the shelf salt balance enhances transformation of water into denser classes.

3. The WIND+ experiment enhances the northward wind-driven export of sea ice, thereby reducing sea ice concentration over the continental shelf. The reduced sea ice cover allows for increased sea ice growth and brine rejection, which increases the salinity on the shelf and thereby enhances surface water mass transformation into the densest classes of shelf water.

The WIND+ and WIND− perturbations shown in Fig. 2 do not allow us to distinguish between these three hypotheses. Thus, we now turn to additional experiments and diagnostics, aiming to rule in, or rule out, each of these hypotheses.

Accepted for publication in *Journal of Climate*. DOI 10.1175/JCLI-D-22-0858.1.

b. Hypothesis 1: Local katabatic winds

We know that local katabatic winds play a key role in opening coastal polynyas where large surface water mass transformation occurs (Fig. 4a; Barthélemy et al. 2012). The first hypothesis we test is whether wind increases in these local katabatic regions are key to driving the increase in DSW export in the WIND+ perturbation. To test this hypothesis we run an additional WIND+$_{\text{no\_local}}$ case, which replicates the WIND+ case, but with no change to the wind in local katabatic regions where DSW is formed (yellow boxes in Fig. 4a). If hypothesis 1 is true, we expect the DSW formation in the WIND+$_{\text{no\_local}}$ simulation to be similar to the CONTROL simulation.

Fig. 4b shows the rate of DSW formation at the four main DSW formation sites. DSW formation is defined as the surface water mass transformation averaged across a fixed range of potential density, calculated following the approach by Newsom et al. (2016). The chosen density range varies between the different DSW formation sites, but is kept fixed across the different perturbations. By averaging across a range of densities, rather than choosing a single density threshold, the diagnostic is less sensitive to the choice of density or year. We average between the densities corresponding to where the CONTROL surface water mass transformation is 30% and 70% of the CONTROL peak transformation (as shown in Fig. S5).

There are large increases in DSW formation at each of the four sites in the WIND+ case (blue bars in Fig. 4b), relative to the CONTROL (black bars). Likewise, we see large decreases in DSW formation in the WIND- case (orange bars). In the WIND+$_{\text{no\_local}}$ case (purple bars), the DSW formation rates increase compared to the CONTROL, despite the lack of wind change over the DSW formation regions. However, the DSW formation increase in the WIND+$_{\text{no\_local}}$ case is 30% less, summed over all formation regions, compared with the DSW formation increase in the WIND+ case. This test indicates that hypothesis 1 – that an increase in local katabatic winds drives the enhanced DSW formation – only partially explains the change in DSW export seen as a response to wind magnitude changes. Fig. 4b suggests that the majority of the changes in DSW export are due to a non-local driver that is outside the DSW formation sites (yellow boxes in Fig. 4a) and widespread across the continental shelf.

Accepted for publication in *Journal of Climate*. DOI 10.1175/JCLI-D-22-0858.1.

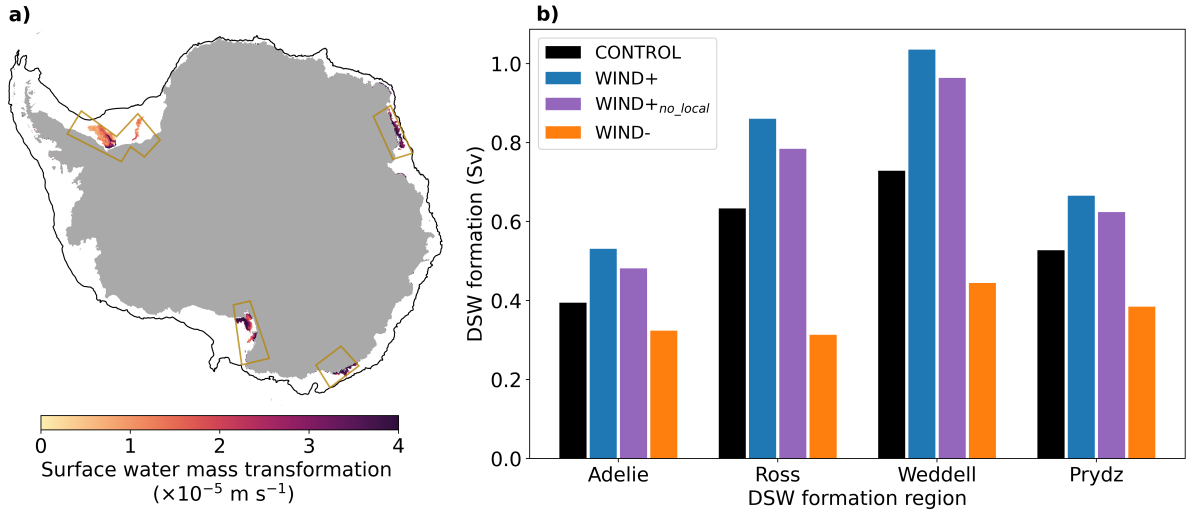

FIG. 4. (a) Surface water mass transformation for the average of the 10 years of the CONTROL simulation. The density threshold used is different for each region and is chosen as the density where the surface water mass transformation is 50% of the peak value (as shown in Fig. S5). Yellow boxes show the four dense water formation sites. (b) Dense water formation rates in each of the four DSW formation regions, averaged over years 6-10, in four different wind perturbation simulations (colors). Dense water formation is calculated by averaging the surface water mass transformation diagnostic between densities corresponding to transformation rates between 30% and 70% of the peak transformation, as shown in Fig. S5.

c. Hypothesis 2: Ekman pumping

Hypothesis 2 suggests that the increase in DSW formation in the WIND+ perturbation is driven by enhanced Ekman upwelling of CDW (i.e. the mechanism described by Stewart and Thompson (2012)). In this scenario, DSW formation increases due to a broad scale increase in the upwelling of relatively salty CDW onto the shelf that enhances transformation of water into denser classes. We analyse this hypothesis by investigating the changes in Ekman pumping along CDW isopycnals. In the CONTROL simulation, warm and salty CDW along the 1000 m isobath is constrained to potential density $\sigma_0 > 27.75\,\mathrm{kg\,m^{-3}}$ (Fig. 5a,b). The depth of this isopycnal experiences little change in the wind perturbation experiments (Fig. 5c), so we can be confident that CDW also remains at potential density $\sigma_0 > 27.75\,\mathrm{kg\,m^{-3}}$ in the wind perturbations. The Ekman-driven upwelling or downwelling along each isopycnal is calculated by binning the total Ekman pumping (due to stresses from both atmosphere and sea ice) into potential density classes using monthly varying

Accepted for publication in *Journal of Climate*. DOI 10.1175/JCLI-D-22-0858.1.

surface potential density. The Ekman pumping is integrated over the area of the wind perturbation region (i.e. south of the blue easterly/westerly dividing line in Fig. 1a). This analysis reveals a net Ekman downwelling within CDW potential density classes $\sigma_0 > 27.75\,\mathrm{kg\,m^{-3}}$ (negative values at high potential densities in Fig. 5d), indicating that these density classes only outcrop close to the Antarctic coastal margin and not in the divergent Ekman upwelling region further north. Furthermore, the Ekman downwelling within CDW potential density classes ($\sigma_0 > 27.75\,\mathrm{kg\,m^{-3}}$) increases (i.e. becomes more negative) in the WIND+ perturbation, with a largely symmetric response in the WIND- perturbation. The lack of Ekman-driven upwelling along CDW isopycnals in the CONTROL and the downwelling anomaly in the WIND+ perturbation suggests that hypothesis 2 is unlikely to explain the enhanced DSW formation in the WIND+ perturbation.

The Ekman pumping analysis is imperfect, due both to the existence of vertical density gradients within the mixed layer and sub-monthly variations in surface density that are not accounted for in the binning method. Isopycnals outcrop into the base of the mixed layer and may be influenced by winds at the surface where the density is less than at the base of the mixed layer. High frequency variability in surface density also may result in the Ekman pumping occurring during short periods of anomalous density being binned incorrectly. Due to these caveats in the Ekman pumping analysis, we will return to test hypothesis 2 more conclusively after we introduce hypothesis 3 in the next section.

d. Hypothesis 3: Sea ice mechanism

We now evaluate the viability of hypothesis 3, which argues that the wind magnitude controls northward sea ice export away from the continental shelf region, and thereby sets the salinity of the shelf region. This mechanism has been investigated previously by Timmermann et al. (2002) and McKee et al. (2011). Freshwater contributions dominate the surface buoyancy fluxes on the Antarctic continental shelf in this model, as shown in Fig. 6a. The net surface heat flux shows a strong seasonal cycle in which summer warming and autumn cooling dominate the surface heat fluxes (solid line in Fig. 6a; noting that in winter and spring the heat fluxes are limited by thick sea ice cover). However, these heat fluxes are overwhelmed by the seasonal cycle of freshwater fluxes due to seasonal sea ice formation (dashed line in Fig. 6a), with melting in spring and summer adding freshwater to the system (thereby decreasing salinity) and sea ice formation in autumn and

Accepted for publication in *Journal of Climate*. DOI 10.1175/JCLI-D-22-0858.1.

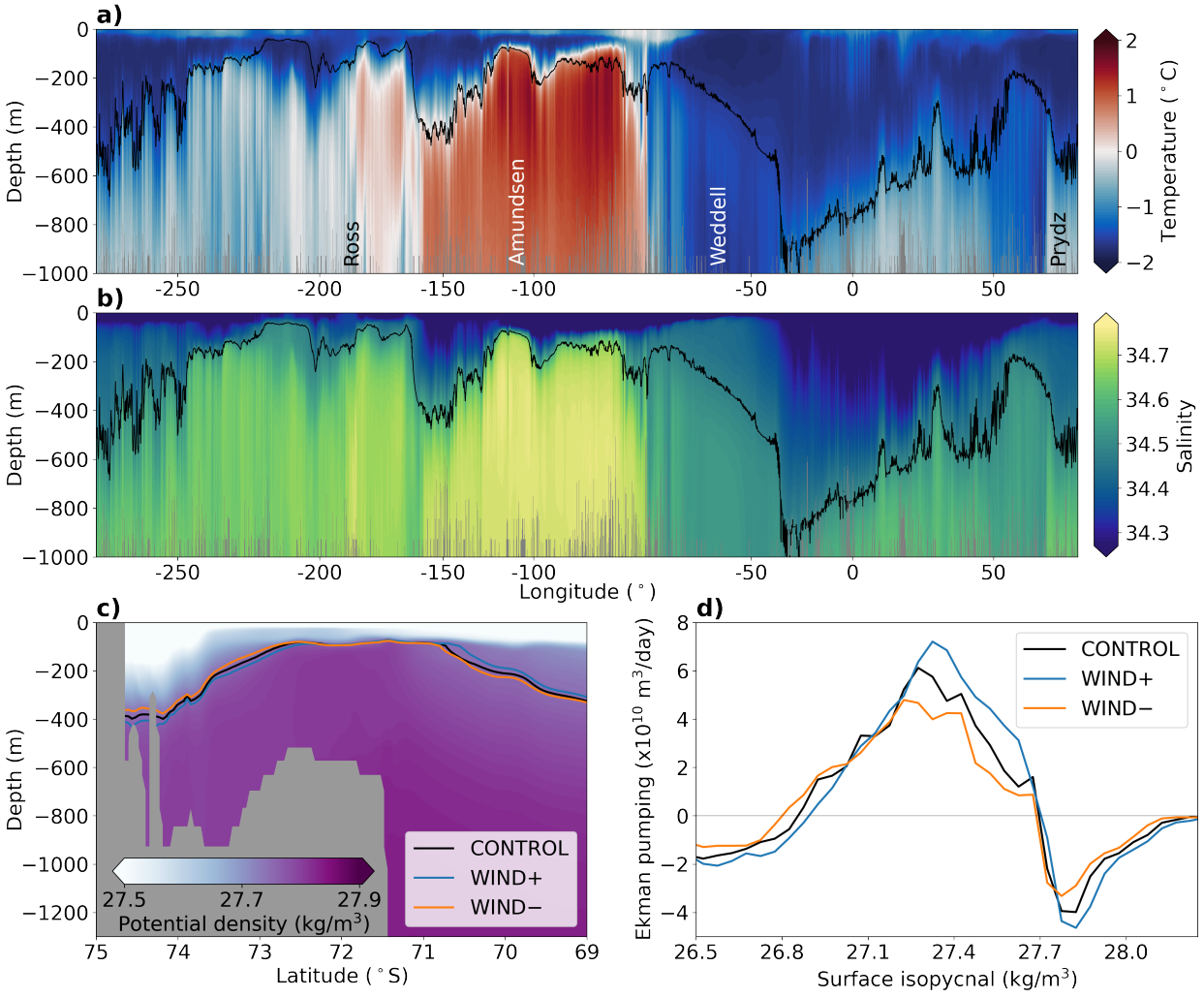

FIG. 5. CONTROL a) vertical profile of temperature and b) salinity following the 1000 m isobath. The location of the 1000 m isobath is shown in Fig. 1. Black contours in a) and b) show the 27.75 kg m^{-3} isopycnal (potential density referenced to the surface). The x-axis is distance along the 1000 m isobath, but labelled with longitude for easier referencing. c) Sample transect of CONTROL potential density referenced to the surface and relative to 1000 kg m^{-3}, averaged between -110 and -115° longitude. Contour lines show the 27.75 kg m^{-3} isopycnal in the wind perturbation simulations. d) Ekman pumping binned into monthly average surface isopycnal classes (0.05 kg m^{-3} bin size), and summed over the wind perturbation zone (south of the blue easterly/westerly dividing line in Fig. 1a). Positive values of Ekman pumping correspond to upwelling. All panels are averaged over years 6-10.

winter increasing the salinity on the continental shelf. The freshwater buoyancy flux signal is an order of magnitude greater than the buoyancy flux from heat, noting that both fluxes have a

Accepted for publication in *Journal of Climate*. DOI 10.1175/JCLI-D-22-0858.1.

very regular seasonal cycle. The buoyancy flux from freshwater is overwhelmingly due to sea ice formation and melt, with a time-invariant offset due to runoff. The precipitation/evaporation and salinity restoring terms used by the model are 1-2 orders of magnitude smaller than the sea ice contribution to the CONTROL buoyancy flux (not shown).

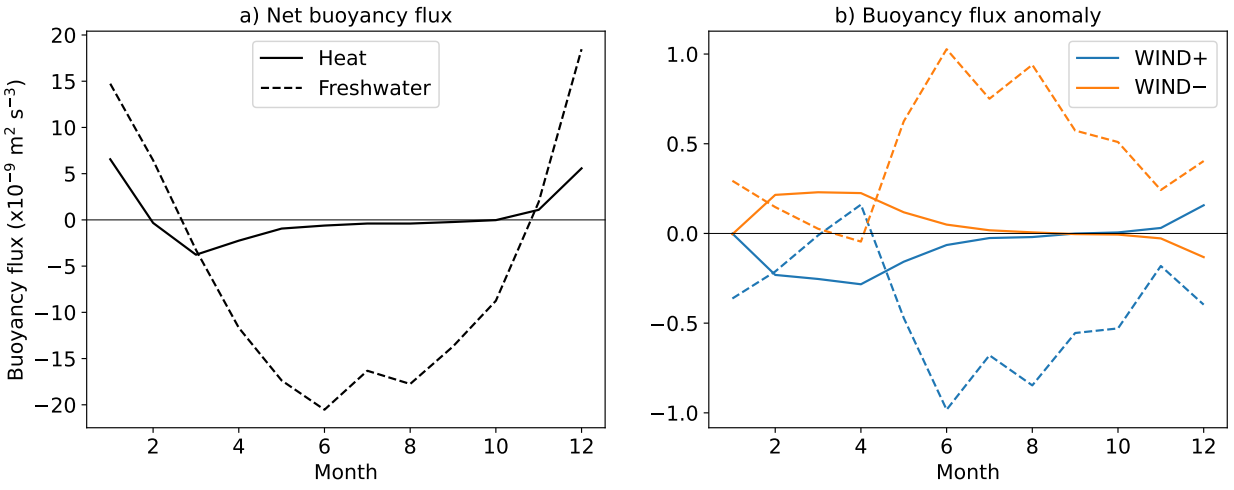

FIG. 6. a) Annual climatology of the net buoyancy flux in the CONTROL simulation, averaged over the Antarctic continental shelf (south of the 1000 m isobath) for model years 6-10. Positive buoyancy fluxes act to increase ocean vertical stratification (stabilizing the water column), whereas negative fluxes act to destabilize the water column. Fluxes are divided into heat (solid) and freshwater (dashed) contributions. b) Buoyancy flux anomaly relative to the CONTROL, for the WIND+ and WIND− cases, averaged over years 6-10. Note the smaller y-axis range in panel b).

The differences in buoyancy fluxes between the CONTROL, WIND+ and WIND− simulations are small compared with the magnitude of the seasonal cycle, so for clarity these fluxes are shown as anomalies from the CONTROL in Fig. 6b. The WIND+ case (blue lines in Fig. 6b) shows a modest surface cooling anomaly, and a stronger surface salinification that is greatest in winter. Sea ice changes dominate (95%) the salinification, but the sea ice buoyancy flux anomaly is damped by ~30% by an opposing buoyancy input from the salinity restoring change (not shown). Conversely, the WIND− case (orange lines) shows both warming and freshening relative to the CONTROL, which is nearly symmetric about the CONTROL with the WIND+ anomalies. These changes are consistent with hypothesis 3. Under increased wind magnitude, the seasonal cycle of sea ice formation and northward export acts to enhance the salinity of the continental shelf region, and

Accepted for publication in *Journal of Climate*. DOI 10.1175/JCLI-D-22-0858.1.

thereby contributes to stronger production of DSW. In a coupled ocean - atmosphere model with no salinity restoring, we would expect this sea ice mechanism to act more strongly than it does in the forced ocean - sea ice model considered here.

If sea ice advection acts to enhance northward freshwater transport and thereby increase shelf salinity, then systematic changes in the pattern of time-averaged sea ice velocities are expected in each perturbation simulation. Fig. 7 shows both the anomalous sea ice thickness and velocity for the two perturbation cases. Northward sea ice advection is clearly enhanced in the WIND+ case, and sea ice thickness on the shelf is reduced (Fig. 7a). Conversely, the WIND− case shows anomalous southward sea ice advection and thicker sea ice on the shelf. These sea ice changes are again consistent with hypothesis 3 in which the wind-driven export of fresh sea ice from the continental shelf increases, resulting in consequent salinification of the shelf region. We now look to additional simulations to provide a more rigorous test of this proposed mechanism.

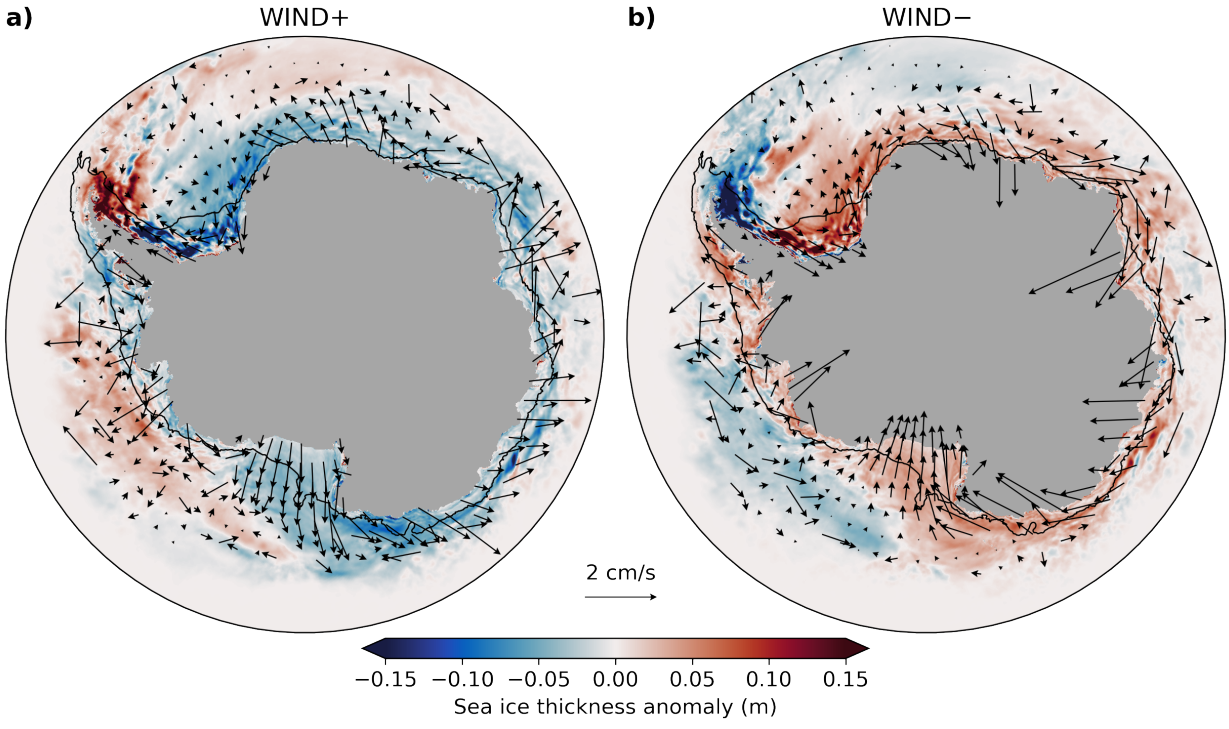

FIG. 7. a) Sea ice thickness (colour) and velocity (arrows) anomalies relative to the CONTROL for the WIND+, and WIND− perturbations, averaged over years 6-10. Velocity anomaly arrows are only shown where the average sea ice concentration > 40% to highlight change near the Antarctic margins.

Accepted for publication in *Journal of Climate*. DOI 10.1175/JCLI-D-22-0858.1.

e. Zonal vs meridional winds

The wind perturbation simulations diagnosed above suggest that, of our three proposed hypotheses, freshwater transport by northward sea ice advection (hypothesis 3) is more consistent with the modelled response than Ekman-driven upwelling (hypothesis 2), while local DSW production from katabatic winds (hypothesis 1) may contribute partially ($\sim 30\%$) to driving the increase in DSW export. However, the evidence presented so far does not categorically eliminate hypothesis 2, while support for hypothesis 3 is not conclusive. Therefore, we now devise two further perturbation simulations to ascertain beyond reasonable doubt the relative effect of Ekman pumping and sea ice advection. These simulations are based on the expectation that southward Ekman upwelling is dominated by the meridional gradient of the zonal winds, while northward sea ice advection is primarily governed by the meridional winds. Along the Antarctic Peninsula, the direction of both the winds and shelf break differ from the rest of the continent (Fig. 1). However, around the majority of the Antarctic margins, we expect these dynamics to hold. The two additional simulations partition the WIND+ perturbation into its zonal (WIND+$_{\text{zonal}}$) and meridional (WIND+$_{\text{merid}}$) components. These additional perturbation simulations allow us to isolate Ekman effects in the WIND+$_{\text{zonal}}$ case, while the WIND+$_{\text{merid}}$ case will primarily affect northward sea ice advection.

The sea level anomaly averaged over the continental shelf in the WIND+$_{\text{merid}}$ case decreases at the same rate as in the WIND+ case, but is offset by a quasi-steady Ekman-driven positive sea level anomaly in the WIND+$_{\text{zonal}}$ experiment (Fig. 8a). This result confirms that the zonal component of the wind perturbation drives the increase in sea level via enhanced onshore Ekman transport, while the meridional component of the wind acts to reduce sea level on the shelf. Furthermore, the increase in DSW export seen in the full WIND+ experiment is entirely explained by the WIND+$_{\text{merid}}$ case, with DSW export unchanged with respect to the CONTROL in the WIND+$_{\text{zonal}}$ case (Fig. 8b).

Therefore, we infer that the increase in salinity due to anomalous northward sea ice advection (Fig. 8c) acts to both enhance the DSW formation and export in the WIND+ experiment, and to induce a steric decrease in sea level over the continental shelf. A small fraction of the sea ice export anomaly is driven by the zonal wind component (dotted line in Fig. 8c), likely due to the non-zonal orientation of the shelf break in some regions (e.g. the Antarctic Peninsula). However the zonal wind component does not contribute to the DSW export anomaly (Fig. 8b). We

Accepted for publication in *Journal of Climate*. DOI 10.1175/JCLI-D-22-0858.1.

hypothesise that this is because the regions where the zonal wind perturbation drives enhanced sea ice export anomaly are not co-located or upstream of the DSW formation sites, and therefore do not contribute to preconditioning the salinity of DSW source waters.

These results are consistent with predictions based on hypothesis 3, in which changes in DSW formation are induced by an increased salinification of the continental shelf waters following enhanced sea ice export due to stronger offshore winds. The WIND+$_{\text{no\_local}}$ experiment showed that the increase in local katabatic winds over the DSW formation sites is also important, but can only explain 30% of the total enhancement of DSW export. The remaining 70% of the increase in DSW export that occurs in the WIND+ experiment (Fig. 2b) is driven by non-local winds increasing the northward export of sea ice away from the continental margins.

f. Impact on shelf temperature

Finally, we discuss the impact of the wind perturbations on the temperature over the continental shelf. We concentrate on the bottom temperature as oceanic basal melting of floating ice shelves is usually driven by warm water intrusions at depth (e.g. Greenbaum et al. 2015; Jenkins et al. 2018). On average, the bottom shelf temperature cools in the WIND+ perturbation (Fig. 9a) and warms in the WIND- perturbation (Fig. 9d). The temperature change in the WIND+ and WIND- perturbations is largely symmetric about the CONTROL, so we focus now on explaining the changes in the WIND+ experiment. The average cooling response in the WIND+ case is consistent with the enhanced southward Ekman transport forcing a downward shift of the water column (Spence et al. 2014). However, there are also hotspots of warming in the WIND+ perturbation, particularly on the western Antarctic Peninsula and between ~30-60°E in East Antarctica.

The individual zonal and meridional wind perturbations nicely separate the effects of coastal Ekman pumping and abyssal overturning circulation change, and help to unravel the spatial heterogeneity in the temperature anomaly in the WIND+ perturbation. In the WIND+$_{\text{zonal}}$ perturbation, the response is dominated by largely coastal-enhanced cooling, as expected from the increased coastal Ekman pumping (Fig. 9b). In contrast, in the WIND+$_{\text{merid}}$ perturbation, there is strong warming on the continental shelf downstream (westward) of most of the DSW formation regions (yellow boxes in Fig. 9c). The temperature change is minimal within the DSW formation regions, because these regions are strongly convecting and waters are already near the surface freezing point

Accepted for publication in *Journal of Climate*. DOI 10.1175/JCLI-D-22-0858.1.

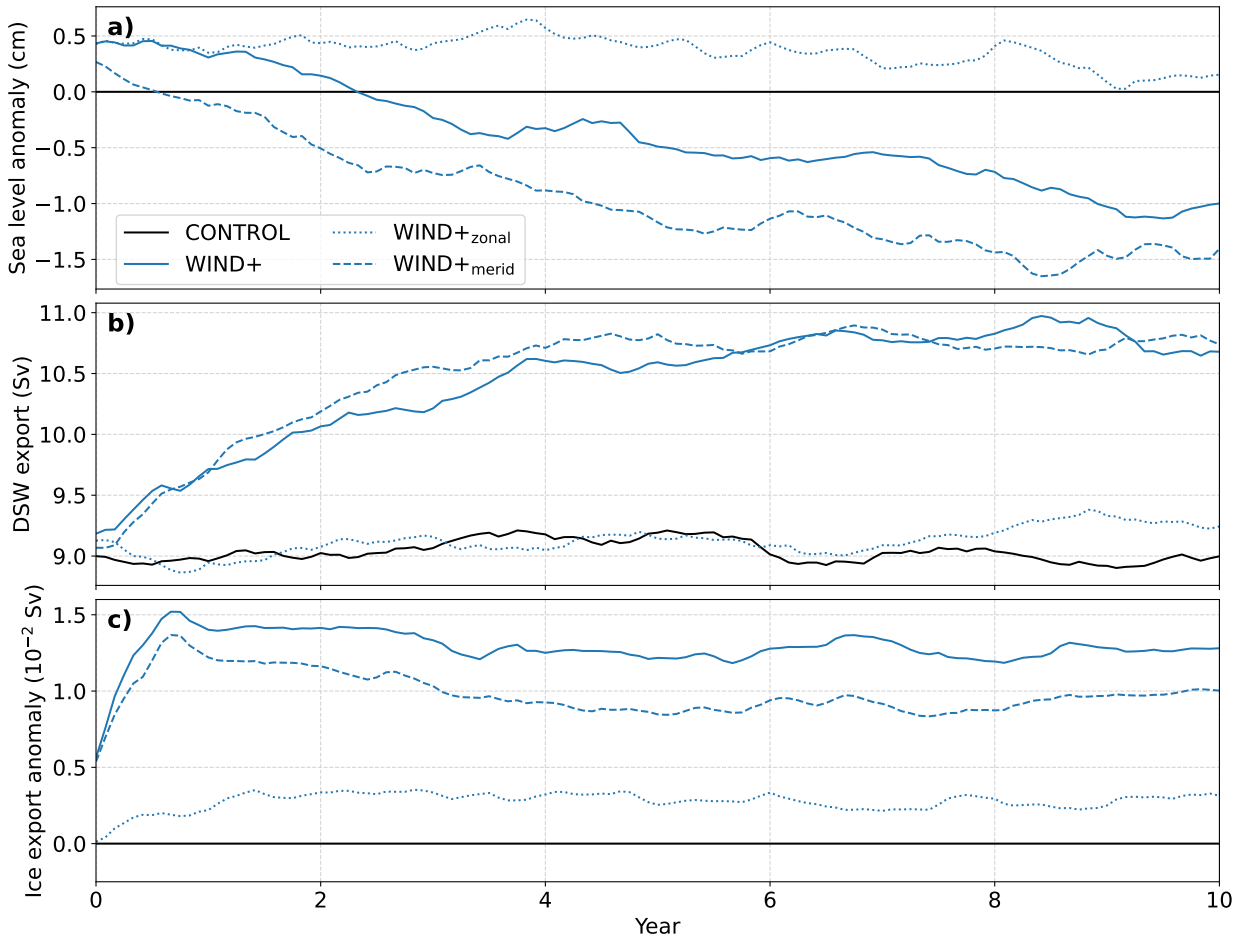

FIG. 8. a) Sea level anomaly relative to the CONTROL, averaged over the continental shelf (south of the 1000 m isobath), for the WIND+, WIND+$_{zonal}$ and WIND+$_{meridional}$ simulations. b) DSW export across the 1000 m isobath for the same simulations. c) Anomaly of equatorward sea ice export across the 1000 m isobath, relative to the CONTROL. All time series have a 12-month rolling mean applied to remove the seasonal cycle.

in the CONTROL simulation. An increase in bottom age, indicative of the increased presence of old CDW waters on the shelf, occurs in the same regions where the temperature warms (Fig. 3a). The warming and aging downstream of the DSW formation sites occurs partly due to the enhanced upward heat transport onto the shelf as the abyssal overturning cell increases (Morrison et al. 2015), and partly due to the redirection of more dense, cold DSW downslope, rather than westward along the continental shelf (Morrison et al. 2023). This additional heat transport onto the shelf is localised at the DSW formation sites (Morrison et al. 2020) and advected downstream by the ASC and coastal currents. The Ross Sea DSW formation region is an exception, with no warming

Accepted for publication in *Journal of Climate*. DOI 10.1175/JCLI-D-22-0858.1.

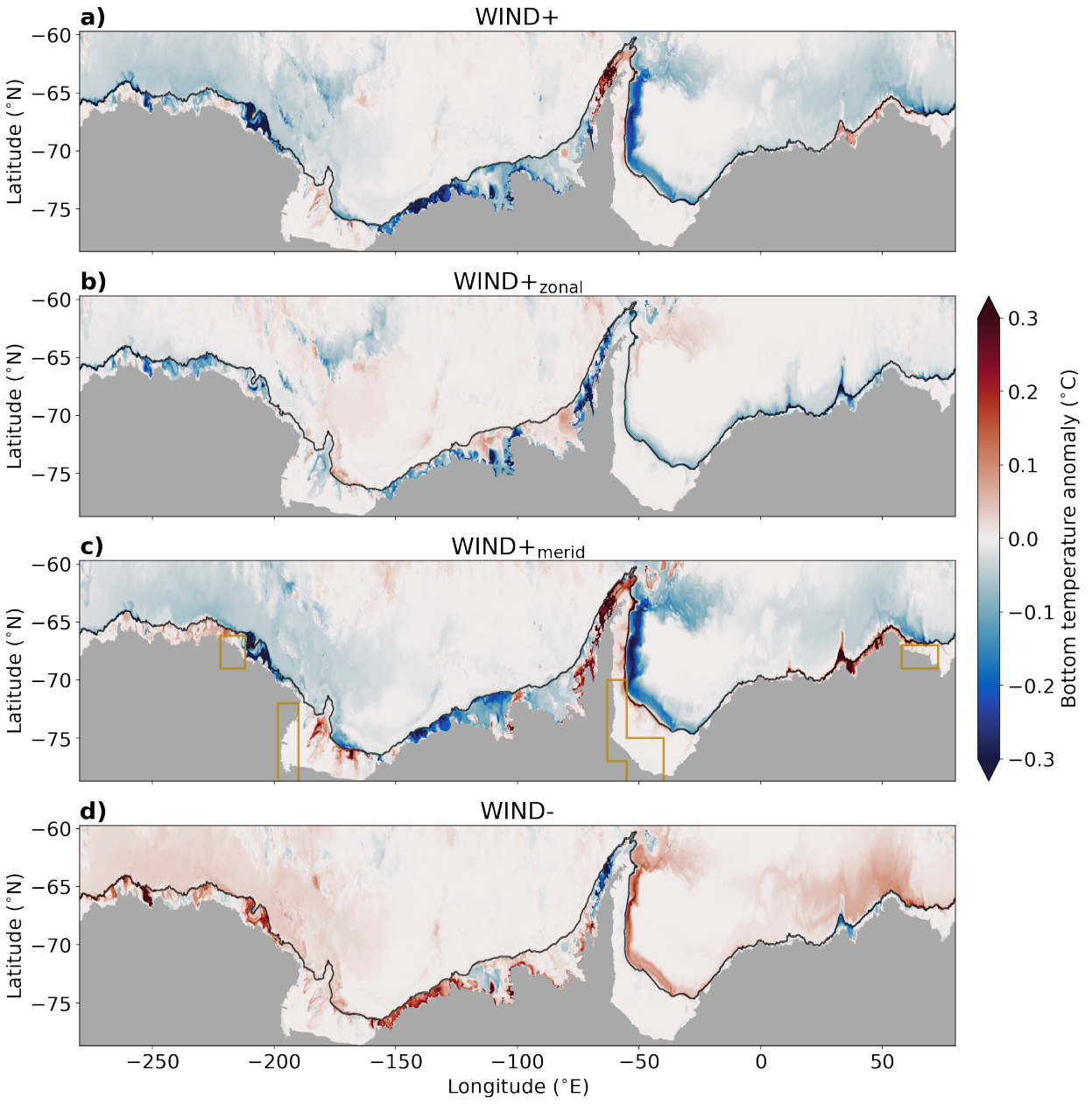

FIG. 9. Bottom temperature anomaly for a) WIND+, b) WIND+$_{zonal}$, c) WIND+$_{merid}$, and d) WIND-, averaged over years 6 to 10 of the simulation. Yellow boxes in c) indicate the DSW formation sites.

occurring downstream, due to the limited connectivity along the shelf past Cape Adare (Dawson et al. 2023). The warming downstream of the DSW formation regions is solely driven by the meridional wind component that is also responsible for the change in the overturning circulation (Fig. 8b).

Accepted for publication in *Journal of Climate*. DOI 10.1175/JCLI-D-22-0858.1.

In contrast, the Amundsen Sea and a localised region near the Cook Depression (~ -205°E) cool in the WIND+$_{merid}$ perturbation (Fig. 9c). These are both regions that have limited connection from upstream DSW formation sites (Dawson et al. 2023). In these regions, the increased meridional wind speed brings colder air and also decreases the sea ice thickness over the continental shelf, leading to enhanced heat loss to the atmosphere, increased sea ice formation and consequently increased mixed layer depths (not shown). However, unlike in the DSW formation regions, the cooled shelf waters in the Amundsen Sea are not dense enough to overflow so there is limited change in the local cross-shelf exchange. Previous model studies of the Amundsen Sea suggest that CDW is brought onto the shelf within troughs by an eastward undercurrent that may strengthen with weaker easterlies (Assmann et al. 2013; Jenkins et al. 2016).

4. Discussion and conclusions

Past work on the response of Antarctic shelf waters and the abyssal overturning to polar winds has presented some disparate dynamical theories, as well as primarily focusing on the response in limited regional domains. In this study, we applied a range of wind perturbations to a global high-resolution ocean - sea ice model, and found that distinct dynamical responses arise from the zonal vs meridional components of the wind forcing (Fig. 10).

Increasing the zonal easterly component of the wind speed drives an enhanced southward Ekman transport in the surface layer, which raises sea level over the continental shelf and deepens isopycnals over the shelf and slope (Fig. 10a). The downward isopycnal movement results in cooling over the continental shelf, as colder surface waters replace warmer waters at depth. This response is consistent with the mechanism found in a lower resolution model by Spence et al. (2014). While the orientation of the shelf break along the western Antarctic Peninsula runs north-east to south-west, rather than east-west, the same mechanism also occurs in this region (Fig. 9b). Southward Ekman transport flows onto the continental shelf (at an angle) and results in cooling along the western Antarctic Peninsula. In the simulations presented here, the zonal easterly winds do not impact the strength of the abyssal overturning circulation. This result is in contrast to past idealised model studies (Stewart and Thompson 2012, 2013) that found that increased easterlies strengthened the abyssal overturning via an Ekman upwelling of Circumpolar Deep Water. We hypothesise that the difference between our results and earlier idealised model studies stems from the different

Accepted for publication in *Journal of Climate*. DOI 10.1175/JCLI-D-22-0858.1.

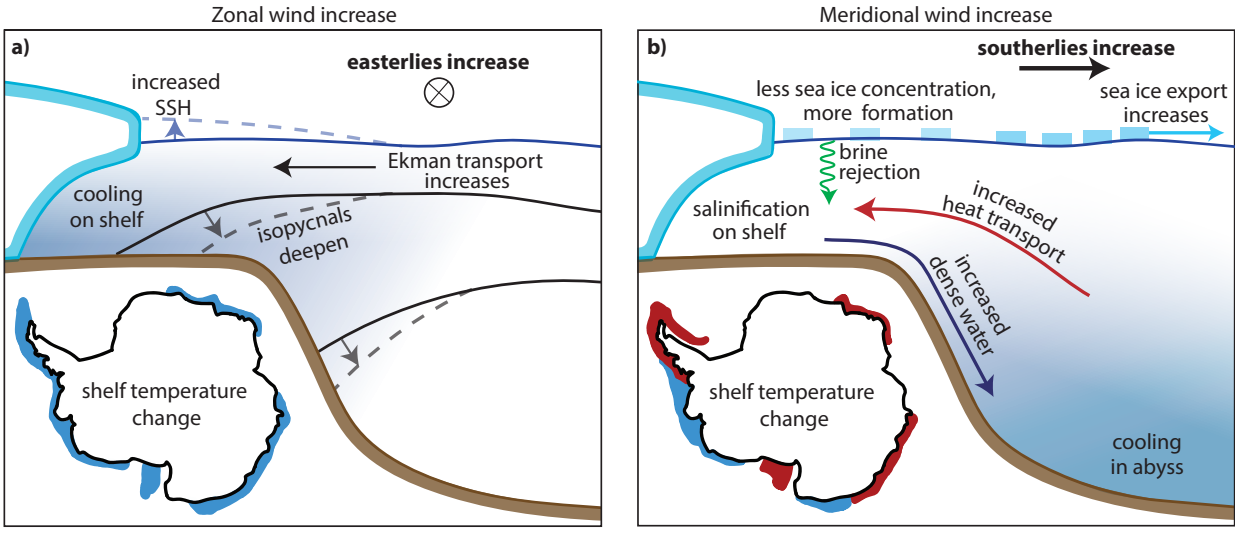

FIG. 10. Schematic showing the controlling dynamics and temperature response to an increase in a) the (easterly) zonal winds and b) the (southerly) meridional winds. a) Increasing the easterly winds drives enhanced southward Ekman transport in the surface layer, which elevates coastal SSH and deepens isopycnals on the shelf and slope. The isopycnal movement results in a cooling on the shelf and limits CDW access to the shelf. b) Increasing the southerly winds enhances sea ice export away from Antarctica, which reduces sea ice concentration over the continental shelf. The increased open water fraction leads to increases in air-sea heat loss, sea ice formation, brine rejection and DSW formation over the continental shelf. The enhancement of the abyssal overturning circulation leads to salinification on the shelf and cooling in the abyss. The bottom temperature response on the continental shelf varies regionally (see inset map), with warming downstream of DSW formation regions.

treatment of surface buoyancy forcing; Dense Shelf Water in this study forms primarily due to elevated salinity driven by sea ice formation, whereas dense water in the model of Stewart and Thompson (2012) is formed via a surface temperature restoring condition. In the more realistic configuration presented here, the Dense Shelf Water is formed primarily via transformation of Lower Circumpolar Deep Water (Morrison et al. 2020), which only outcrops close to the Antarctic coast and therefore is less sensitive to the Ekman upwelling-favourable winds further north (Fig. 5).

In contrast, the increased meridional wind perturbation does strengthen the abyssal overturning circulation, through a sea ice advection feedback mechanism (Fig. 10b). Enhancing the offshore meridional wind speed increases the northward export of sea ice, resulting in decreased sea ice thickness over the continental shelf. The reduction in sea ice coverage increases the ocean heat loss

Accepted for publication in *Journal of Climate*. DOI 10.1175/JCLI-D-22-0858.1.

and therefore the rate of sea ice formation. The resultant increased brine rejection enhances the formation of Dense Shelf Water and the abyssal overturning circulation. We find that enhancement of local katabatic winds over the localised DSW formation sites only drives 30% of the total DSW increase, with the majority of the DSW increase driven by non-local meridional winds. This sea ice - abyssal overturning mechanism has been identified previously in the Weddell (Timmermann et al. 2002; McKee et al. 2011; Hazel and Stewart 2020) and Ross Seas (Dinniman et al. 2018). However we find that this mechanism holds in all four of the Dense Shelf Water formation sites around Antarctica, including the Adélie coast and Cape Darnley. Increasing the meridional winds causes warming at depth over a large part of the continental shelf. This warming is partly due to the heat advection feedback associated with the enhanced overturning circulation bringing more warm Circumpolar Deep Water onto the shelf and partly due to the preferential down-slope, rather than along-slope pathway of cold waters when they are more dense (Morrison et al. 2023). The Amundsen Sea is sufficiently far from an upstream Dense Shelf Water formation site (i.e. the Weddell Sea), that it is not affected by this mechanism and undergoes cooling instead.

A caveat of this study is that the model does not include the coupled feedback of dynamic ice shelf melt (e.g. Naughten et al. 2022). Regions that warm in response to an increase in the abyssal overturning circulation (Fig. 9c and Fig. 10b) would subsequently drive an increase in basal melt, which, when advected downstream (Dawson et al. 2023), could be a negative feedback on the overturning circulation and warming anomaly identified here. We also have not considered seasonal changes in the wind speed, as have been reported in reanalysis trends (Hazel and Stewart 2019) and CMIP6 projections (Neme et al. 2022).

CMIP6 projections suggest that future Southern Hemisphere polar wind changes may be dominated by a decrease in the zonal wind speed, with a smaller decrease in the meridional wind speed (Neme et al. 2022). Our results suggest that such a future wind change would contribute to a weakening of the abyssal cell and an overall warming anomaly of the shelf waters around the Antarctic margins (essentially, the inverse of changes suggested schematically in Fig. 10). The strong easterly winds in the present-day climate act to buffer ice shelves from warm Circumpolar Deep Water, via the wind-driven southward Ekman transport of cold, upper ocean waters. This buffering effect is likely to diminish in the future. The magnitude of future wind-driven warming at the Antarctic margins may be of comparable magnitude to meltwater-driven temperature changes

Accepted for publication in *Journal of Climate*. DOI 10.1175/JCLI-D-22-0858.1.

(e.g. Moorman et al. 2020; Li et al. 2023), though future work is needed to further understand the coupled ocean - ice shelf response in the context of other changes in Antarctic climate.

Accepted for publication in *Journal of Climate*. DOI 10.1175/JCLI-D-22-0858.1.

Acknowledgments. This was an open collaborative project conducted using github, and a full history of project contributions is available here: https://github.com/adele157/easterlies-collaborative-project. This research was undertaken on the National Computational Infrastructure (NCI) in Canberra, Australia, which is supported by the Australian Government. The authors thank the Consortium for Ocean – Sea Ice Modelling in Australia (COSIMA; http://www.cosima.org.au) for making the ACCESS-OM2 suite of models available. AKM was supported by the Australian Research Council (ARC) DECRA Fellowship DE170100184. WGCH was supported by the ARC Discovery Project DP190100494. PS was supported by Australian Research Council (ARC) Future Fellowship FT190100413. This research was also supported by the ARC Special Research Initiative, Australian Centre for Excellence in Antarctic Science (Project Number SR200100008). We thank Jan-Erik Tesdal for useful comments on an early draft.

All authors contributed to the formulation, analysis and writing of this paper; author order was partly decided by a game of rock-paper-scissors.

Data availability statement. The model output for the simulations presented in this paper is available in the COSIMA data collection, available from https://doi.org/10.4225/41/5a2dc8543105a (COSIMA, 2019). Data for the different simulations is tagged under experiment names as follows: CONTROL (`01deg_jra55v13_ryf9091`), WIND+ (`01deg_jra55v13_ryf9091_easterlies_up10`), WIND- (`01deg_jra55v13_ryf9091_easterlies_down10`), WIND+$_{\text{zonal}}$ (`01deg_jra55v13_ryf9091_easterlies_up10_zonal`) and WIND+$_{\text{merid}}$ (`01deg_jra55v13_ryf9091_easterlies_up10_meridional`). Analysis code is available at https://github.com/adele157/easterlies-collaborative-project/tree/master/notebooks/.

References

Assmann, K. M., A. Jenkins, D. R. Shoosmith, D. P. Walker, S. S. Jacobs, and K. W. Nicholls, 2013: Variability of Circumpolar Deep Water transport onto the Amundsen Sea continental shelf through a shelf break trough. *J. Geophys. Res.*, **118**, 6603–6620.

Barthélemy, A., H. Goosse, P. Mathiot, and T. Fichefet, 2012: Inclusion of a katabatic wind correction in a coarse-resolution global coupled climate model. *Ocean Modell.*, **48**, 45–54.

Accepted for publication in *Journal of Climate*. DOI 10.1175/JCLI-D-22-0858.1.

Beadling, R. L., and Coauthors, 2022: Importance of the Antarctic Slope Current in the Southern Ocean response to ice sheet melt and wind stress change. *J. Geophys. Res.*, **127**, e2021JC017 608.

Bowen, M. M., D. Fernandez, A. Forcen-Vazquez, A. L. Gordon, B. Huber, P. Castagno, and P. Falco, 2021: The role of tides in bottom water export from the western Ross Sea. *Sci. Rep.*, **11**, 2246.

Bracegirdle, T. J., W. M. Connolley, and J. Turner, 2008: Antarctic climate change over the twenty first century. *J. Geophys. Res.*, **113**, D03 103.

Bromwich, D. H., and D. D. Kurtz, 1984: Katabatic wind forcing of the Terra Nova Bay polynya. *J. Geophys. Res.*, **89**, 3561–3572.

Caillet, J., N. C. Jourdain, P. Mathiot, H. H. Hellmer, and J. Mouginot, 2023: Drivers and reversibility of abrupt ocean state transitions in the Amundsen Sea, Antarctica. *J. Geophys. Res.*, **128**, e2022JC018 929.

Dawson, H., A. K. Morrison, M. H. England, and V. Tamsitt, 2023: Pathways and timescales of connectivity around the Antarctic continental shelf . *J. Geophys. Res.*, **128**, e2022JC018 962.

Dinniman, M. S., J. M. Klinck, E. E. Hofmann, and W. O. S. Jr., 2018: Effects of projected changes in wind, atmospheric temperature, and freshwater inflow on the Ross Sea. *J. Clim.*, **31**, 1619–1635.

Fogt, R. L., and D. H. Bromwich, 2006: Decadal variability of the ENSO teleconnection to the high-latitude South Pacific governed by coupling with the Southern Annular Mode. *J. Clim.*, **19**, 979–997.

Frankcombe, L., P. Spence, A. M. Hogg, M. H. England, and S. M. Griffies, 2013: Sea level changes forced by Southern Ocean winds. *Geophys. Res. Lett.*, **40**, 5565–5825.

Greenbaum, J. S., and Coauthors, 2015: Ocean access to a cavity beneath Totten Glacier in East Antarctica. *Nat. Geosci.*, **8**, 294–298.

Griffies, S. M., 2012: Elements of the Modular Ocean Model (MOM). *GFDL Ocean Group Tech. Rep*, **7**, 47.

Accepted for publication in *Journal of Climate*. DOI 10.1175/JCLI-D-22-0858.1.

Griffies, S. M., and Coauthors, 2014: An assessment of global and regional sea level for years 1993–2007 in a suite of interannual CORE-II simulations. *Ocean Modell.*, **78**, 35–89.

Hazel, J. E., and A. L. Stewart, 2019: Are the near-Antarctic easterly winds weakening in response to enhancement of the Southern Annular Mode? *J. Clim.*, **32**, 1895–1918.

Hazel, J. E., and A. L. Stewart, 2020: Bistability of the Filchner-Ronne ice shelf cavity circulation and basal melt. *J. Geophys. Res.*, **125**, e2019JC015 848.

Holland, P. R., T. J. Bracegirdle, P. Dutrieux, A. Jenkins, and E. J. Steig, 2019: West Antarctic ice loss influenced by internal climate variability and anthropogenic forcing. *Nat. Geosci.*, **12**, 718–724.

Hunke, E., W. Lipscomb, A. Turner, N. Jeffery, and S. Elliott, 2015: CICE: The Los Alamos sea ice model documentation and software user's manual version 5 (Tech. Rep. LA-CC-06–012). *Los Alamos, NM: Los Alamos National Laboratory*.

Jenkins, A., P. Dutrieux, S. Jacobs, E. Steig, H. Gudmundsson, J. Smith, and K. Heywood, 2016: Decadal ocean forcing and Antarctic Ice Sheet response: Lessons from the Amundsen Sea. *Oceanography*, **29**, 106–117.

Jenkins, A., D. Shoosmith, P. Dutrieux, S. Jacobs, T. W. Kim, S. H. Lee, H. K. Ha, and S. Stammerjohn, 2018: West Antarctic Ice Sheet retreat in the Amundsen Sea driven by decadal oceanic variability. *Nat. Geosci.*, **11**, 733–738.

Kida, S., 2011: The impact of open oceanic processes on the Antarctic Bottom Water outflows. *J. Phys. Oceanogr.*, **41**, 1941–1957.

Kiss, A. E., and Coauthors, 2020: ACCESS-OM2: A global ocean-sea ice model at three resolutions. *Geosci. Model Dev.*, **13**, 401–442.

Lago, V., and M. H. England, 2019: Projected slowdown of Antarctic Bottom Water formation in response to amplified meltwater contributions. *J. Clim.*, **32**, 6319–6335.

Li, Q., M. H. England, A. M. Hogg, S. R. Rintoul, and A. K. Morrison, 2023: Abyssal ocean overturning slowdown and warming driven by Antarctic meltwater. *Nature*, **615**, 841–847.

Accepted for publication in *Journal of Climate*. DOI 10.1175/JCLI-D-22-0858.1.

Locarnini, M., and Coauthors, 2018: World Ocean Atlas 2018, Volume 1: Temperature. *NOAA Atlas NESDIS 82*.

Massom, R. A., P. Harris, K. J. Michael, and M. Potter, 1998: The distribution and formative processes of latent-heat polynyas in East Antarctica. *Ann. Glaciol.*, **27**, 420–426.

Mathiot, P., B. Barnier, H. Gallée, J. M. Molines, J. Le Sommer, M. Juza, and T. Penduff, 2010: Introducing katabatic winds in global ERA40 fields to simulate their impacts on the Southern Ocean and sea-ice. *Ocean Modell.*, **35**, 146–160.

McKee, D. C., X. Yuan, A. L. Gordon, B. A. Huber, and Z. Dong, 2011: Climate impact on interannual variability of Weddell Sea Bottom Water. *J. Geophys. Res.*, **116**, C05 020.

Meier, W. N., F. Fetterer, M. Savoie, S. Mallory, R. Duerr, and J. Stroeve, 2017: NOAA/NSIDC climate data record of passive microwave sea ice concentration, version 3. *NSIDC: National Snow and Ice Data Center*, https://doi.org/10.7265/N59P2ZTG.

Moorman, R., A. K. Morrison, and A. M. Hogg, 2020: Thermal responses to Antarctic ice shelf melt in an eddy rich global ocean–sea-ice model. *J. Clim.*, **33**, 6599–6620.

Morrison, A., M. H. England, A. M. Hogg, and A. E. Kiss, 2023: Weddell Sea control of ocean temperature variability on the western Antarctic Peninsula. *Geophys. Res. Lett.*, Submitted, https://doi.org/10.22541/essoar.167591098.80596021/v1.

Morrison, A., A. M. Hogg, M. H. England, and P. Spence, 2020: Warm Circumpolar Deep Water transport toward Antarctica driven by local dense water export in canyons. *Sci. Adv.*, **6**, eaav2516.

Morrison, A. K., M. H. England, and A. M. Hogg, 2015: Response of Southern Ocean convection and abyssal overturning to surface buoyancy perturbations. *J. Clim.*, **28**, 4263–4278.

Naughten, K. A., P. R. Holland, P. Dutrieux, S. Kimura, D. T. Bett, and A. Jenkins, 2022: Simulated twentieth-century ocean warming in the Amundsen Sea, West Antarctica. *Geophys. Res. Lett.*, **49**, e2021GL094 566.

Neme, J., M. H. England, and A. M. Hogg, 2022: Projected changes of surface winds over the Antarctic continental margin. *Geophys. Res. Lett.*, **49**, e2022GL098 820.

Accepted for publication in *Journal of Climate*. DOI 10.1175/JCLI-D-22-0858.1.

Newsom, E. R., C. M. Bitz, F. O. Bryan, R. Abernathey, and P. R. Gent, 2016: Southern Ocean deep circulation and heat uptake in a high-resolution climate model. *J. Clim.*, **29**, 2597–2619.

Orsi, A. H., W. M. Smethie, and J. L. Bullister, 2002: On the total input of Antarctic waters to the deep ocean: A preliminary estimate from chlorofluorocarbon measurements. *J. Geophys. Res.*, **107**, 3122.

Palóczy, A., S. T. Gille, and J. L. McClean, 2018: Oceanic heat delivery to the Antarctic continental shelf: large-scale, low-frequency variability. *J. Geophys. Res.*, **123**, 7678–7701.

Pellichero, V., J.-B. Sallée, C. C. Chapman, and S. M. Downes, 2018: The Southern Ocean meridional overturning in the sea-ice sector is driven by freshwater fluxes. *Nat. Commun.*, **9**, 1789.

Peng, G., W. N. Meier, D. Scott, and M. Savoie, 2013: A long-term and reproducible passive microwave sea ice concentration data record for climate studies and monitoring. *Earth Syst. Sci. Data*, **5**, 311–318.

Raphael, M. N., and Coauthors, 2016: The Amundsen Sea Low: variability, change, and impact on Antarctic climate. *Bull. Amer. Meteor.*, **97**, 111–121.

Schmidt, C., A. K. Morrison, and M. H. England, 2023: Wind- and sea-ice-driven interannual variability of Antarctic Bottom Water formation. *J. Geophys. Res.*, Submitted, https://doi.org/10.22541/essoar.167768108.88472952/v1.

Schmidtko, S., K. J. Heywood, A. F. Thompson, and S. Aoki, 2014: Multidecadal warming of Antarctic waters. *Science*, **346**, 1227–1231.

Silvano, A., and Coauthors, 2020: Recent recovery of Antarctic Bottom Water formation in the Ross Sea driven by climate anomalies. *Nat. Geosci.*, **13**, 780–786.

Silvano, A., and Coauthors, 2022: Baroclinic ocean response to climate forcing regulates decadal variability of ice-shelf melting in the Amundsen Sea. *Geophys. Res. Lett.*, **49**.

Solodoch, A., A. L. Stewart, A. M. Hogg, A. K. Morrison, A. E. Kiss, A. F. Thompson, S. G. Purkey, and L. Cimoli, 2022: How does Antarctic Bottom Water cross the Southern Ocean? *Geophys. Res. Lett.*, **49**, e2021GL097 211.

Accepted for publication in *Journal of Climate*. DOI 10.1175/JCLI-D-22-0858.1.

Spence, P., S. M. Griffies, M. H. England, A. M. Hogg, O. A. Saenko, and N. C. Jourdain, 2014: Rapid subsurface warming and circulation changes of Antarctic coastal waters by poleward shifting winds. *Geophys. Res. Lett.*, **41**, 4601–4610.

Stewart, A. L., and A. F. Thompson, 2012: Sensitivity of the ocean's deep overturning circulation to easterly Antarctic winds. *Geophys. Res. Lett.*, **39**, L18 604.

Stewart, A. L., and A. F. Thompson, 2013: Connecting Antarctic cross-slope exchange with Southern Ocean overturning. *J. Phys. Oceanogr.*, **43**, 1453–1471.

Stewart, K. D., and Coauthors, 2020: JRA55-do-based repeat year forcing datasets for driving ocean–sea-ice models. *Ocean Model.*, **147**, 101 557.

Tesdal, J.-E., G. A. MacGilchrist, R. L. Beadling, S. M. Griffies, J. P. Krasting, and P. Durack, 2023: Revisiting interior water mass responses to surface forcing changes and the subsequent effects on overturning in the Southern Ocean. *J. Geophys. Res.*, **128**, e2022JC019 105.

Thompson, A. F., A. L. Stewart, P. Spence, and K. J. Heywood, 2018: The Antarctic Slope Current in a changing climate. *Rev. Geophys.*, **56**, 741–770.

Timmermann, R., H. H. Hellmer, and A. Beckmann, 2002: Simulations of ice-ocean dynamics in the Weddell Sea 2. Interannual variability 1985–1993. *J. Geophys. Res.*, **107**, 3025.

Tsujino, H., and Coauthors, 2018: JRA-55 based surface dataset for driving ocean–sea-ice models (JRA55-do). *Ocean Modell.*, **130**, 79–139.

Wang, Q., S. Danilov, E. Fahrbach, J. Schröter, and T. Jung, 2012: On the impact of wind forcing on the seasonal variability of Weddell Sea Bottom Water transport. *Geophys. Res. Lett.*, **39**, L06 603.

Zweng, M., and Coauthors, 2019: World Ocean Atlas 2018, Volume 2: Salinity. *NOAA Atlas NESDIS 82*.

Accepted for publication in *Journal of Climate*. DOI 10.1175/JCLI-D-22-0858.1.